THE JOURNAL OF PHYSICAL CHEMISTRY B

Article

pubs.acs.org/JPCB

Delineation of the Unbinding Pathway of α-Conotoxin ImI from the α7 Nicotinic Acetylcholine Receptor

Rilei Yu,[†,‡] Quentin Kaas,[†,‡] and David J. Craik*[,†]

[†]Division of Chemistry and Structural Biology, Institute for Molecular Bioscience, The University of Queensland, Brisbane, Queensland 4072, Australia

Supporting Information

ABSTRACT: α-Conotoxins potently and specifically inhibit isoforms of nicotinic acetylcholine receptors (nAChRs) and are used as molecular probes and as drugs or drug leads. Interactions occurring during binding and unbinding events are linked to binding kinetics, and knowledge of these interactions could help in the development of α-conotoxins as drugs. Here, the unbinding process for the prototypical α-conotoxin ImI/α7-nAChR system was investigated theoretically, and three exit routes were identified using random accelerated molecular dynamics simulations. The route involving the smallest conformation perturbation was further divided into three subpathways, which were studied using steered molecular dynamics simulations. Of the three subpathways, two had better experimental support and lower potential of mean force, indicating that they might be sampled more frequently. Additionally, these subpathways were supported by previous experimental studies. Several pairwise interactions, including a cation-π interaction and charge and hydrogen bond interactions, were identified as potentially playing important roles in the unbinding event.

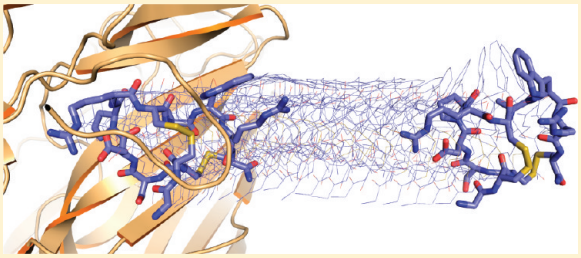

1. INTRODUCTION

Conotoxins are disulfide-rich peptides isolated from the venom of marine snails belonging to the genus *Conus*.[1] α-Conotoxins are one of the largest families of conotoxins and are characterized by their potent and specific inhibition of nicotinic acetylcholine receptors (nAChRs).[2,3] Most α-conotoxins comprise 12−22 residues and two disulfide bonds. The spacing between the Cys residues defines two loop regions, the length of which is used to classify α-conotoxins into several subfamilies. One of the shortest α-conotoxins, ImI, belongs to the 4/3 subfamily and potently inhibits α7- and α3β2-nAChRs.[4−6] The specificity and potency of α-conotoxins, as well as their rigid and well-defined structures,[7] make them valuable molecular probes as well as drugs or drug leads.[8−10] The structure and activities of ImI have been extensively investigated, both in experimental and modeling studies.[11−19] The wealth of experimental information on the ImI/α7-nAChR system provides an ideal case for a theoretical investigation of the mechanism of action of α-conotoxins.

nAChRs are ligand gated ion channels that are involved in synapse transmission and have a range of physiological roles.[20,21] These receptors have been implicated in several disorders and diseases and, as such, are considered significant targets for drug design.[20,21] nAChRs are composed of several subunits (α1−10, β1−4, γ, δ, and ε), which assemble to form pentamer subtypes that have different physiological roles. For example, the α7-nAChR homopentamer is essential for memory and learning.[22−24]

The cryo-electron microscopy structure of *Torpedo marmorata* nAChR at 4 Å resolution, depicted in Figure 1, reveals that each subunit comprises an extracellular domain, a transmembrane domain and an intracellular domain.[25] The ligand binding site is located at the interface between adjacent subunits on the extracellular domain.[26] This binding site comprises three loops, designated as the A-, B-, and C-loops in Figure 1. Because it has not yet been possible to determine a crystallographic structure of the nAChR, the acetylcholine binding protein (AChBP) has been used as a surrogate to carry out rational drug design.[27,28] AChBP and the extracellular domain of the nAChR both bind acetylcholine and adopt similar structures. The crystal structures of AChBP complexed with different ligands suggest that the conformation of the C-loop varies significantly with the ligand size.[29] The C-loop of the receptor adopts a closed conformation when it interacts with agonists, whereas competitive antagonists stabilize the C-loop in an open conformation.

The crystal structure of AChBP and the cryo-electron microscopy structure of *Torpedo marmorata* muscle-type nAChR have been used as templates for modeling several Cys-loop receptors, including nAChR, 5-hydroxytryptamine type 3 (5-HT_3), γ-aminobutyric acid (GABA), and glycine receptors.[30−35] Ligand docking and molecular dynamics simulations have been performed on the cryo-electron

Received: February 10, 2012
Revised: May 8, 2012
Published: May 9, 2012

dx.doi.org/10.1021/jp301352d | J. Phys. Chem. B 2012, 116, 6097−6105

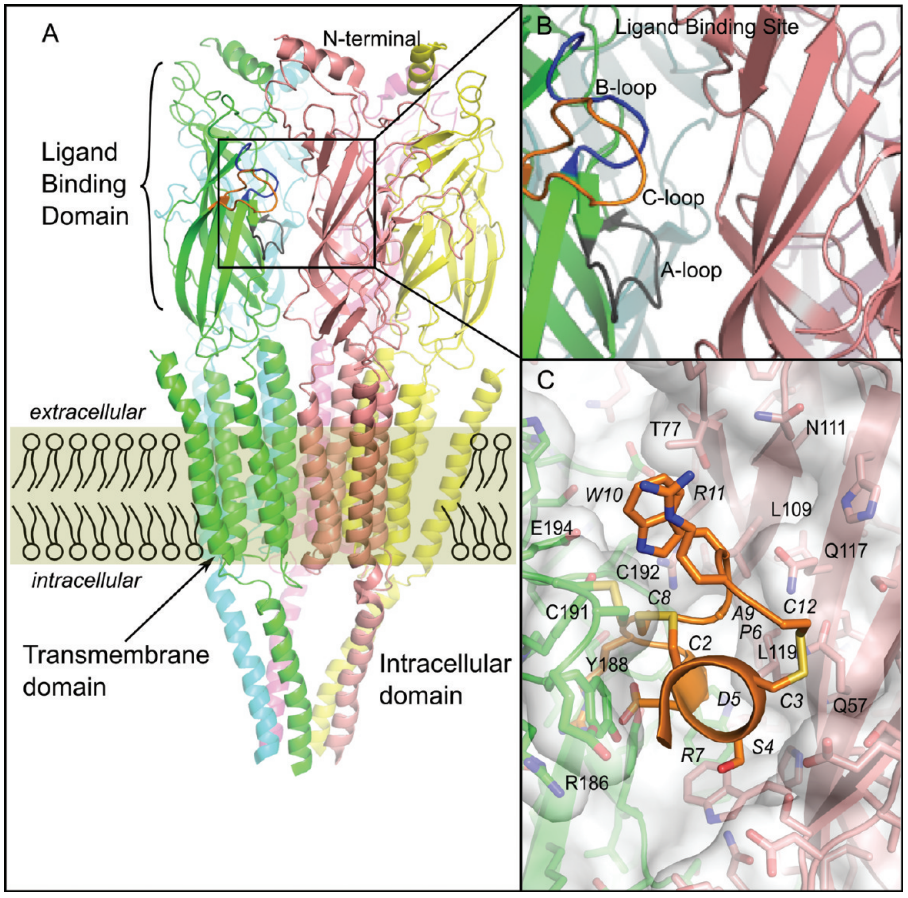

Figure 1. Structure of the nicotinic acetylcholine receptor (nAChR) and its ligand binding site. (A) The nAChR is composed of five subunits, each comprising three domains: an extracellular domain, a transmembrane domain, and an intracellular domain. The EM structure of *Torpedo marmorata* nAChR (PDB identifier 2bg9) was used in this figure. (B) The nAChR binding site comprises the A-loop (gray), B-loop (blue), and C-loop (orange) of the principal subunit (green) and β-strands of the complementary subunit (light pink). (C) Molecular model of the interaction between conotoxin ImI (orange) and α7-nAChR (green and pink).[19] This model was created using a combination of molecular dynamic simulations and homology modeling based on three-dimensional crystallographic structures of AChBP and of a single α1-nAChR subunit.[19]

microscopy structure of the nAChR or on homology models of other Cys-loop receptors to understand the mechanism and conformational changes associated with ligand binding and channel gating.[36−42] In our previous study, a model of the complex between α-conotoxin ImI and the extracellular domain of the α7-nAChR was obtained based on homology modeling and molecular dynamics (MD) simulation (Figure 1C).[19] This model provides insight into the binding modes and binding determinants of α-conotoxins interacting with nAChR, and it explains the effect of more than 30 mutations performed experimentally. Here, we investigated the possible involvement of other residues in interactions that occur during unbinding of the toxin, and therefore potentially influence the unbinding kinetics. Unbinding events typically occur on a millisecond time scale, which is out of reach for conventional MD simulations. To overcome this limitation, random accelerated molecular dynamics (RAMD) simulations[43] and steered molecular dynamics (SMD) simulations[44,45] were developed to study unbinding events that occur over this time scale. SMD has only been applied in a handful of publications to protein/peptide or protein/protein complexes, including major histocompatibility complex/peptide,[46,47] antibody/antigen,[48] and barnase/barstar[49] complexes. Our simulations predict the most probable unbinding pathways and specific interactions, strengthening our understanding of the molecular interactions between α-conotoxins and nAChRs. This new knowledge can be used in future rational drug design studies to improve the specificity and kinetics of conotoxin variants.

2. METHODS

2.1. Molecular Dynamics Simulation. A model of the complex between ImI and α7-nAChR was built as described previously.[19] This complex was solvated into a TIP3P water box with dimensions of 101 × 99 × 103 Å^3. The system was set at physiological ionic strength and neutralized by adding 53 Na^+ and 42 Cl^- ions using VMD.[50] The system was minimized using 1000 steps of conjugated-gradient minimization. After minimization, the system was gradually heated from 0 to 300 K over 50 ps using Langevin MD with a damping coefficient of 1 ps^{-1}. A constant pressure of 1 atm was maintained using the Langevin piston method.[51] The system was equilibrated using 5 ns NPT MD at 300 K. The electrostatic interactions between noncovalent atoms were computed with particle-mesh Ewald (PME)[52] method with a distance cutoff of 10 Å. MD simulations were performed using the NAMD 2.7 package[53] and the CHARMM22 forcefield.[54]

2.2. Random Accelerated Molecular Dynamics Simulation. The egress routes of ImI from the extracellular domain of the α7-nAChR were explored using RAMD simulations.[43] The routes of the ligand were searched by applying a randomly

dx.doi.org/10.1021/jp301352d | J. Phys. Chem. B 2012, 116, 6097−6105

orientated force to the center of mass of the ligand.[43] The magnitude of the force was kept constant over the simulation, but the orientation of the applied force was changed according to the following algorithm: (1) the direction and sense of the force was kept constant during N simulation steps; (2) after N steps, if the center of mass of the ligand covered a distance less than r_{min}, then the direction was randomly changed, otherwise it was conserved for the following N steps. We used the algorithm implemented in the NAMD 2.7 package and described by Vashisth and Abrams.[55] The parameters r_{min}, N, and the acceleration were kept at their default values of 0.002 Å, 10 steps, and 0.25 kcal/mol·Å·amu, respectively. Fifty RAMD simulations were performed, and trajectories in which ImI successfully unbound were clustered using VMD.[50]

2.3. Steered Molecular Dynamics Simulations. In a series of 48 SMD simulations, the center of mass of ImI was pulled over 20 Å at constant velocity along the three subpathways identified by RAMD simulations using a soft elastic force with a spring constant of 10 kcal·mol^{-1}·Å^{-2}. The simulation time of each SMD simulation was about 2 ns. Large velocities can induce unrealistic deformation of the molecules, but small velocities prolong simulation time. In this study, a pulling rate of 10 Å·ns^{-1} was used to simulate the unbinding event at the nanosecond time scale along the three subpathways. This pulling speed was found to be slow enough to reasonably sample unbinding trajectories.[56] To prevent the receptor from drifting during the pulling process, the Cα atoms of V109 and Q117 were restrained using a harmonic potential of 5 kcal/mol·Å. Residues V109 and Q117 are located on the same β-strand, which had a stable conformation in our previous MD study of α7-nAChR.[19] For each studied unbinding pathway, SMD simulations were performed 16 times with different velocity seeds. The SMD simulations were performed with NAMD 2.7 package and the CHARMM22 forcefield.[53,54]

2.4. Potential of Mean Force (PMF). The PMF was estimated for each SMD trajectory using Jarzynski's equation[57−59]

$$\langle e^{-\beta w}\rangle = e^{-\beta \Delta G} \quad (1)$$

where w is the work, ΔG is the free energy or PMF, and $\beta = 1/k_B T$ in which k_B is the Boltzmann constant and T is the temperature. The angular brackets denote ensemble average. Jarzynski's equation establishes a relationship between free energy and the work distribution of nonequilibrium processes.[57−59]

The external work w performed on ImI was calculated by integrating the pulling force F along the SMD trajectories, using

$$w(t) = v \int_0^t F(t)\mathrm{d}t \quad (2)$$

where v is the pulling velocity (10 Å^2/ns).

F was calculated using the following equation:

$$F(t) = k(vt - (\mathbf{r}(t) - \mathbf{r}_0)\mathbf{n}) \quad (3)$$

where k is the spring constant (k = 10 kcal/mol·Å^2), $\mathbf{n}$ is the vector of the pulling force, and $\mathbf{r}(t)$ and $\mathbf{r}_0$ are the positions of the center of mass of ImI at time t and at initial time.

Similar to a previous study of the interaction between acetylcholine and α7-nAChR,[60] the PMF was computed by using Jarzynski's equation or by using three simplification or extrapolation methods, i.e., second order cumulant expansion, linear extrapolation, and cumulative integral extrapolation.

By assuming a Gaussian distribution of the work values, eq 1 can be simplified using the second order cumulant expansion[57]

$$\Delta G = \langle w\rangle - \beta/2(\langle w^2\rangle - \langle w\rangle^2) \quad (4)$$

where $\langle w\rangle$ is the mean work over all trajectories, and $\langle w^2\rangle - \langle w\rangle^2$ is the square standard deviation of the work distribution.

Yterberg and Zuckerman developed two extrapolation methods of the PMF based on subsample averaging technique to correct for limited sampling of the work distribution.[61] The linear extrapolation method is based on the observation that increasing the size of the subsamples causes a linear decrease of the estimated PMF toward the experimental value. In the cumulative integral extrapolation method, an integral that converges toward the PMF is defined. This integral depends on the number of work values in the subsamples and is solved numerically. The cumulative integral requires 5- to 40-fold less work values to estimate the PMF with the same accuracy than the nonextrapolated Jarzynski's equation.[61] The two extrapolation methods are implemented in the scripts from Ytreberg and Zuckerman.[61]

To assess the impact on the PMF of the pulling speed and of the maximal distance of ImI from its initial position, ten SMD simulations were performed on PW1b with reduced pulling velocity (5 Å·ns^{-1}), and ten simulations were carried out until ImI reached a distance of 30 Å from its starting position. With these additional simulations, a total of 68 SMD simulations were performed.

2.5. Buried Surface Area. The buried surface area of the complex was calculated using the Molsurf[62] algorithm with a probe radius of 1.4 Å. The buried surface area values were averaged over the 16 SMD simulations performed for each subpathway.

3. RESULTS AND DISCUSSION

Exit routes of ImI from the extracellular domain of α7-nAChR were determined using RAMD, and the most probable pathway was predicted to be in the direction opposite to the C-loop. RAMD simulations have been used extensively to study the exit pathways of small molecules and protein ligands from their binding sites.[43,63−65] In this study, 50 RAMD simulations were performed, and the 34 trajectories in which ImI successfully unbound from its binding site were clustered into three pathways, noted PW1, PW2, and PW3. These pathways are depicted in Figure 2. The global directions of PW1, PW2, and PW3 could be described as opposite to the C-loop, toward the membrane, and facing the C-loop, respectively. Statistics on the frequency, structural deformation, and length of the simulations are provided in Table 1. PW1 was the most frequently sampled pathway, with the number of PW2 simulations half that of PW1, and PW3 sampled only five times out of 34 simulations. As well as being the most frequently sampled pathway, compared to the other two pathways, PW1 was associated with smaller conformational changes within the ImI ligand. For example, in contrast to the root-mean square deviation (rmsd) variations within ImI of 1.25 Å for PW1, the maximal rmsd of ImI was more than 2 Å in simulations corresponding to PW2, which is large considering the small size of the ImI backbone. The maximal backbone rmsd of the receptor was over 4 Å in PW3 simulations, mainly accounting for a large change of conformation of the C-loop. Overall, PW3 is the least probable pathway because (1) it was sampled by the smallest number of simulations; (2) it displayed the largest conformational

dx.doi.org/10.1021/jp301352d | J. Phys. Chem. B 2012, 116, 6097−6105

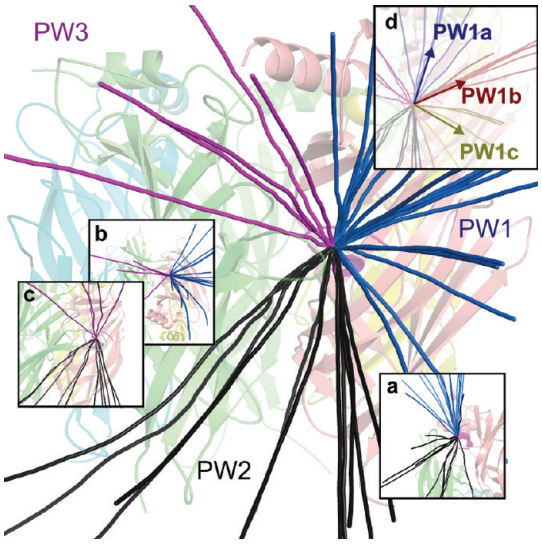

Figure 2. Locations of conotoxin ImI during random accelerated molecular dynamics (RAMD) simulations of the unbinding process from the α7-nAChR, showing clustering in pathways. The positions of the center of mass of ImI in 34 RAMD simulations are represented as lines. The RAMD trajectories were clustered in three pathways denoted PW1, PW2, and PW3. The subpanels a, b, and c show different views that illustrate the separation between PW1 and PW2, PW1 and PW3, and PW2 and PW3, respectively. PW1 was divided into three subpathways noted PW1a, PW1b, and PW1c, the global directions of which are shown in subpanel d. The initial conformation of the α7-nAChR is shown in the background. The RAMD simulations were performed using the NAMD 2.7 package,[53] the CHARMM22 forcefield,[54] and the algorithm of Vashisth and Abrams.[55] Clustering was performed using VMD.[50].

Table 1. Statistics on Unbinding Pathways of Conotoxin ImI from α7-nAChR Studied by Random Accelerated Molecular Dynamics

pathway[a]	frequency[b]	length[c]	rmsd Re[d]	rmsd Lig[e]
PW1	18	2863 (850)	1.27 (0.76)	1.25 (0.40)
PW1a	7	3620 (1133)	1.62 (1.04)	1.42 (0.53)
PW1b	6	2265 (216)	0.81 (0.36)	1.01 (0.21)
PW1c	5	2507 (1208)	1.32 (0.85)	1.31 (0.42)
PW2	11	6063 (3010)	2.11 (1.52)	2.11 (0.42)
PW3	5	8828 (3626)	4.62 (1.08)	1.69 (0.45)

[a]Thirty-four random accelerated molecular dynamics (RAMD) simulations were clustered in three pathways PW1, PW2 and PW3; PW1 was further divided into three subpathways denoted PW1a, PW1b and PW1c. The RAMD simulations were performed using the NAMD 2.7 package,[53] the CHARMM22 forcefield,[54] and the RAMD algorithm of Vashisth and Abrams.[55] Clustering was performed using VMD.[50] [b]Number of RAMD trajectories clustered in each pathway and subpathway. [c]Number of simulation steps needed for ImI to exit the binding site. The number of steps was averaged over the RAMD simulations in each pathway, and the standard deviation of the number of steps is provided between parentheses. [d]Maximum rmsd (Å) of receptor backbone from the starting conformation. The rmsd was computed for the two subunits that form the binding site and averaged over the RAMD simulations in each pathway. The standard deviation of the maximal rmsd is between parentheses. [e]Maximum rmsd (Å) of ImI backbone of ImI from the starting conformation. The rmsd was averaged over the RAMD simulations in each pathway, and the standard deviation of the maximal rmsd is between parentheses.

perturbation of the receptor; and (3) it had the longest simulation time (Table 1). PW1 simulations only required half the number of simulation steps as PW2 simulations to unbind ImI, and the deformations of both the receptor and ImI were smaller for PW1 than PW2. These properties suggest that PW1 is the most probable pathway. As shown in Figure 2, PW1 was further divided into three subpathways, denoted PW1a, PW1b, and PW1c, the global directions of which are 45° apart. The number of RAMD simulations, the conformational change, and the number of simulation steps required to exit the binding site were similar for the three subpathways (Table 1).

The conformational changes occurring in the binding site and in ImI for the three subpathways were more thoroughly investigated by generating 48 SMD simulations. The distance between the initial position and the position at different times during the simulation was used as the reaction coordinate in the following discussion. At the end of the simulation, the center of mass of ImI was 20 Å from the starting location, and at this point, ImI was out of the binding pocket but still in contact with the α7-nAChR. The ten additional SMD simulations performed until ImI reached 30 Å from the starting position indicate that these remaining interactions at 20 Å are negligible, as discussed below. The C-loop of acetylcholine receptors has been suggested to adopt different conformations to accommodate ligands of various sizes in the binding site.[29] The evolution of the distance between the tip of the C-loop and a position in the β-sheet from the complementary subunit is shown in Figure 3 and was used to evaluate the change of conformation of the C-loop during the SMD simulations. PW1a and PW1c simulations displayed similar behavior, as in both cases the binding site underwent a transient but large opening, and ultimately, the C-loop tended to adopt a conformation similar to the starting conformation. PW1b simulations were substantially different from those of the two other subpathways as, at the beginning of PW1b simulations, the C-loop was closer to the β-sheet of the binding site and then moved back to its initial conformation. Interestingly, the difference between the maximum and minimum opening was similar in the three subpathways, at ~9 Å. This indicates that the conformational variation of the binding site was similar in the three subpathways and cannot be used to assess the relative probability of ImI taking any of the exit routes. Because of its disulfide cross-linking and small size, ImI has a highly stable scaffold, and in all SMD simulations, the maximum rmsd of ImI from its initial conformation was <1 Å (Figure S1, Supporting Information).

Four methods derived from Jarzynski's equality were used to calculate the PMF of PW1b, and the two extrapolated methods showed good agreement with the standard Jarzynski's equation. The evolution of the PMF at different reaction coordinates is shown in Figure 4. PMF values calculated using the cumulant expansion of the Jarzynski's equality were substantially different from those calculated using other methods, which produced similar curves. The discrepancy between the cumulant expansion and the other methods probably originates from the non-Gaussian distribution of the work values in our simulations, which is a condition of applicability of the cumulant expansion.[57] The PMF curve computed with the standard Jarzynski's equation displayed a higher slope than the extrapolated method at the end of the simulation, when ImI has left the binding pocket. Extrapolation based methods are expected to be more efficient at estimating the PMF in the present study because the large size of the ImI/α7-nAChR system prevented efficient sampling of the accessible conformational space.[56,61] The cumulative extrapolation integral and

dx.doi.org/10.1021/jp301352d | J. Phys. Chem. B 2012, 116, 6097−6105

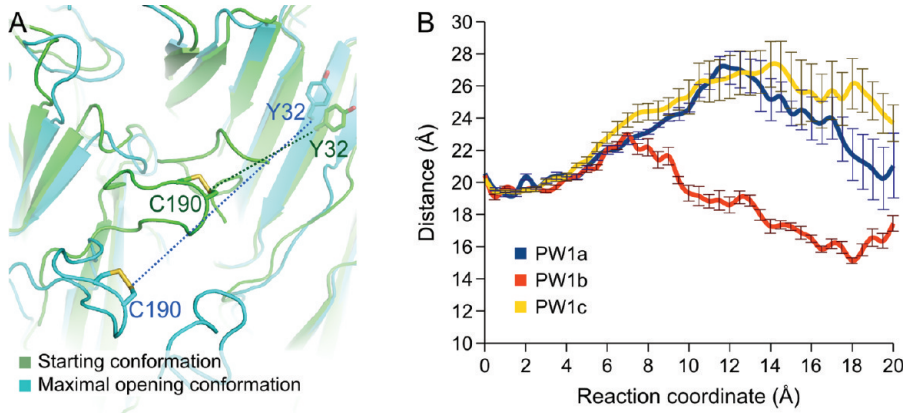

Figure 3. Change of conformation of the C-loop in the unbinding subpathways PW1a, PW1b, and PW1c of the conotoxin ImI from α7-nAChR during steered molecular dynamics (SMD) simulations. Sixteen SMD simulations were performed for each subpathway using NAMD 2.7 package,[53] the CHARMM22 forcefield,[54] and a pulling rate of 10 Å·ns^{-1}. (A) Superimposition of the starting conformation and the conformation displaying the maximal opening of the C-loop in one PW1c simulation. The distance between the sulfur atom of the Cys-190 side chain, located at the tip of the C-loop, and the α carbon of Tyr-32, located in the β-sheet of the complementary subunit is used to characterize the opening of the C-loop. (B) Evolution of the Cys-190 to Tyr-32 distance during the SMD simulations. The reaction coordinate used on the x-axis is the distance between the initial position and the position during the simulation of the center of mass of ImI. The Cys-190 to Tyr-32 distance was averaged over 16 SMD simulations in each subpathway, and error bars represent standard deviations.

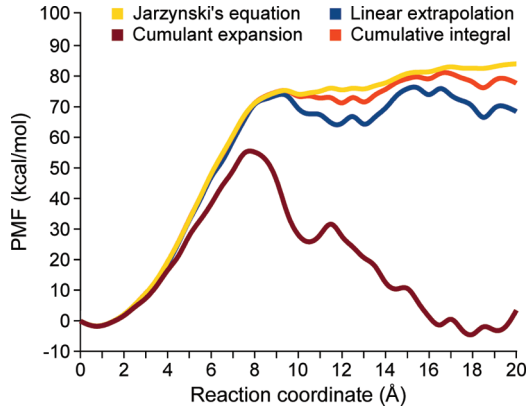

Figure 4. Comparison of methods to compute the potential of mean force (PMF) as applied to steered molecular dynamics (SMD) simulations of the unbinding subpathway PW1b of conotoxin ImI from the α7-nAChR. Four methods were employed to compute the PMF: plain Jarzynski's equation (yellow),[57,58] cumulant expansion (brown),[57] linear extrapolation (blue),[61] and cumulative integral extrapolation (red).[61] The PMFs were computed using 16 SMD simulations for each subpathway. The reaction coordinate used on the x-axis is the distance between the initial position and the position during the simulation of the center of mass of ImI.

linear extrapolation methods were further used to compute the PMF of PW1a and PW1c.

To investigate the energy profile of the unbinding of ImI via each subpathway, the PMF was computed for all SMD simulations, and this analysis showed that PW1a is less probable than the other subpathways. As shown in Figure 5, the PMFs of all subpathways initially increased rapidly and then increased more slowly. From 1−8 Å, the PMF of the three subpathways had similar profiles and increased with a steep slope, suggesting that, during the initial stage, the unbinding of ImI was impeded by similar interactions with the receptor in all subpathways. During this first stage, the buried surface area between ImI and α7-nAChR was approximately 1500 Å^2 in each subpathway (Figure 6), which is comparable to the initial buried surface area (1600 Å^2). For PW1b, a dramatic change of slope of the PMF occurred around 8 Å (Figure 5). At this distance, the buried surface area decreased rapidly (Figure 6), and the C-loop started to occlude the binding pocket, indicating that ImI leaves the binding pocket. A change of slope of the PMF also occurred around 8 Å for the PW1c simulations but the system required less energy to reach this reaction coordinate in PW1c simulations than in PW1b simulations. For PW1a, the change of slope occurred much further away, at around 12 Å, and required larger energies than the other subpathways. Therefore, PW1a is probably the less naturally sampled subpathway. In a previous study, Zhang and colleagues showed that the preferential unbinding pathway of acetylcholine from α7-nAChR is parallel to the membrane, corresponding to PW1c in our study.[60] As shown in Figure 5, the PMF of PW1c is substantially lower at 9 Å than that of PW1b, but they reach the same level at 20 Å. Between 9 and 20 Å, the larger conformation change of the C-loop and the larger number of interactions in PW1c probably contribute to the decrease of the energy difference with PW1b.

The possible influence of pulling speed and pulling distance on the variation of PMF was analyzed for pathway PW1b, and the results are shown in Figure S3, Supporting Information. With a slower pulling velocity (Figure S3A, Supporting Information), the dramatic change of slope of the PMF was also observed around 8 Å, indicating that the pulling velocity did not introduce significant distortion that could influence qualitative investigation of the unbinding event. At a greater distance than 20 Å (Figure S3B, Supporting Information), ImI completely dissociated from the receptor, and this dissociation had no major impact on the PMF, which increases with a similar slope to that observed between 10 and 20 Å.

Ultimately, if the simulations were carried out long enough and slowly enough to allow the interacting molecules to thoroughly sample their accessible conformational space, then the simulations and the PMFs should converge toward equilibrium states and thermodynamic unbinding free energies, respectively.[56] Nevertheless, the computational limitations associated with large biological systems have been shown to impede the statistical convergence of nonequilibium SMD simulations in estimating binding free energies.[46,49] Indeed, the

dx.doi.org/10.1021/jp301352d | J. Phys. Chem. B 2012, 116, 6097−6105

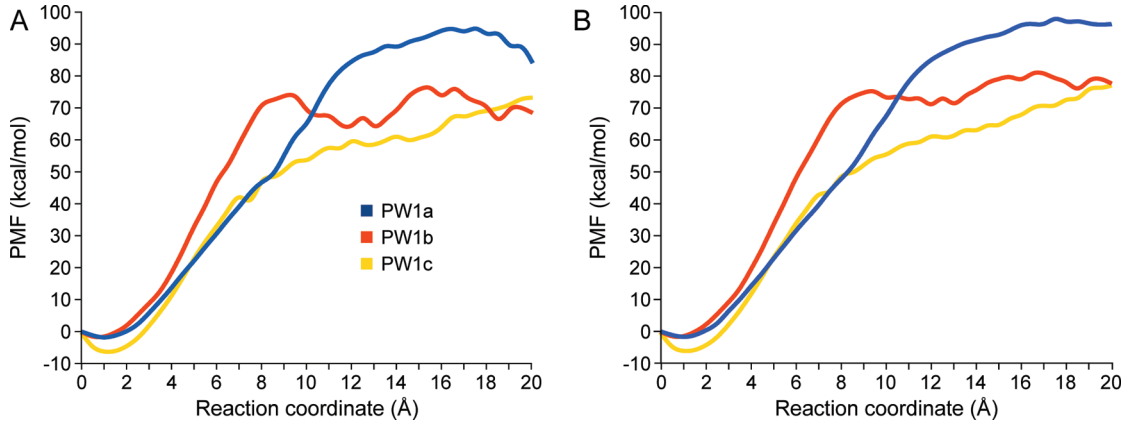

Figure 5. Potential of mean force (PMF) calculated for the unbinding of ImI from the α7-nAChR in subpathways PW1a, PW1b, and PW1c during steered molecular dynamics (SMD) simulations. (A) PMF computed using the linear extrapolation integral. (B) PMF computed using the cumulative integral extrapolation. The PMFs were computed using 16 SMD simulations for each subpathway. The reaction coordinate used on the *x*-axis is the distance between the initial position and the position during the simulation of the center of mass of ImI.

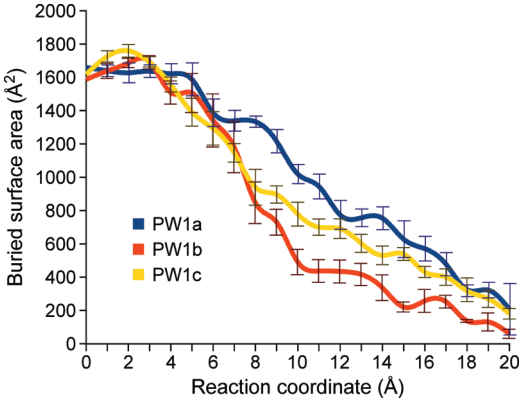

Figure 6. Variation of the buried surface area between conotoxin ImI and α7-nAChR in the subpathways PW1a, PW1b, and PW1c sampled by steered molecular dynamics (SMD) simulations. The buried-surface area was averaged over 16 SMD simulations, and error bars represent standard deviations. The reaction coordinate used on the *x*-axis is the distance between the initial position and the position during the simulation of the center of mass of ImI.

binding free energy of ImI estimated using the PMF in PW1b was of about −70 kcal/mol, which is substantially different from the −9 kcal/mol experimental binding free energy.[5] The order of magnitude of the difference between PMF and binding free energy in our study is comparable to that found in a study of TcR/peptide/MHC systems.[46] Two main explanations for this difference encountered in large biological systems have been proposed: the low sampling of the energy landscape perpendicular to the pulling direction[49] and the influence of the pulling restraints on the translational and rotational entropies of the molecules.[46] Lowering the pulling speed has been shown to improve agreement with experimental data,[49] and we indeed found a slight improvement by performing ten SMD simulations along PW1b with half the original speed (Figure S3, Supporting Information). Importantly, the change of pulling speed did not affect the distance at which the PMF trends to a dramatically changed slope, and the identification of this distance was the main purpose of computing the PMF.

A comparison of the residues involved in each subpathway with previous mutational studies supports the hypothesis that PW1a is probably less sampled than the other two subpathways. Figure 7 shows the evolution of the involvement of the receptor positions at the interface. Most of the receptor residues involved in the subpathways are already in contact with ImI in the bound state. At 10 Å, roughly corresponding to the change of slope of the PMF in the three subpathways, the majority of the binding site positions do not interact anymore with ImI, with the exception of residues at the tip of the C-loop, including Y188, C190, C191, and Y195. Three residues located at the periphery of the binding site, S34, Q161, and E162, were shared among two or three subpathways, and their interactions with ImI are therefore potentially important to interpret kinetic data. Some positions were specific for one subpathway, and experimental mutational studies can be used to evaluate the relative probabilities of the subpathways. The specific positions associated with each subpathway are K76, T77, W154, and E193 for PW1a; S113 and H115 for PW1b; and D164 for PW1c. Figure 7 shows that K76 is located in the middle of the route taken by ImI in PW1a, but the mutation of K76 to alanine has no significant effect experimentally,[15] suggesting that PW1a has low probability. As discussed previously, the PMF of PW1a is also higher than those of the two other subpathways, and this difference is consistent with a lower probability of PW1a. Residues that were mutated to alanine and had no effect cannot be in highly sampled pathways, and therefore, the experimental effect of the K76A mutation indicates that PW1a has a low probability. Conversely, T77 and W154 are specific to PW1a but their mutation to alanine has been shown experimentally to impact the binding of ImI. We propose that the mutation of these two positions could have an indirect effect on the receptor activity by modifying the conformation of the binding site without directly interacting with ImI. S113 and H115 significantly influence the binding of ImI experimentally and are both involved in PW1b. D164 is part of PW1c and experimentally has an effect on the binding of ImI. Single point mutations can cause conformational changes of nearby residues, and therefore, mutations that have experimental effects cannot be used to support the higher probability of pathways. Therefore, despite all experimentally studied positions in PW1b and PW1c showing a difference of activity upon mutation, the experimental data cannot be used to rank the probability of PW1b and PW1c. Nevertheless, the theoretical PMF of PW1c is constantly lower than that of

dx.doi.org/10.1021/jp301352d | J. Phys. Chem. B 2012, 116, 6097−6105

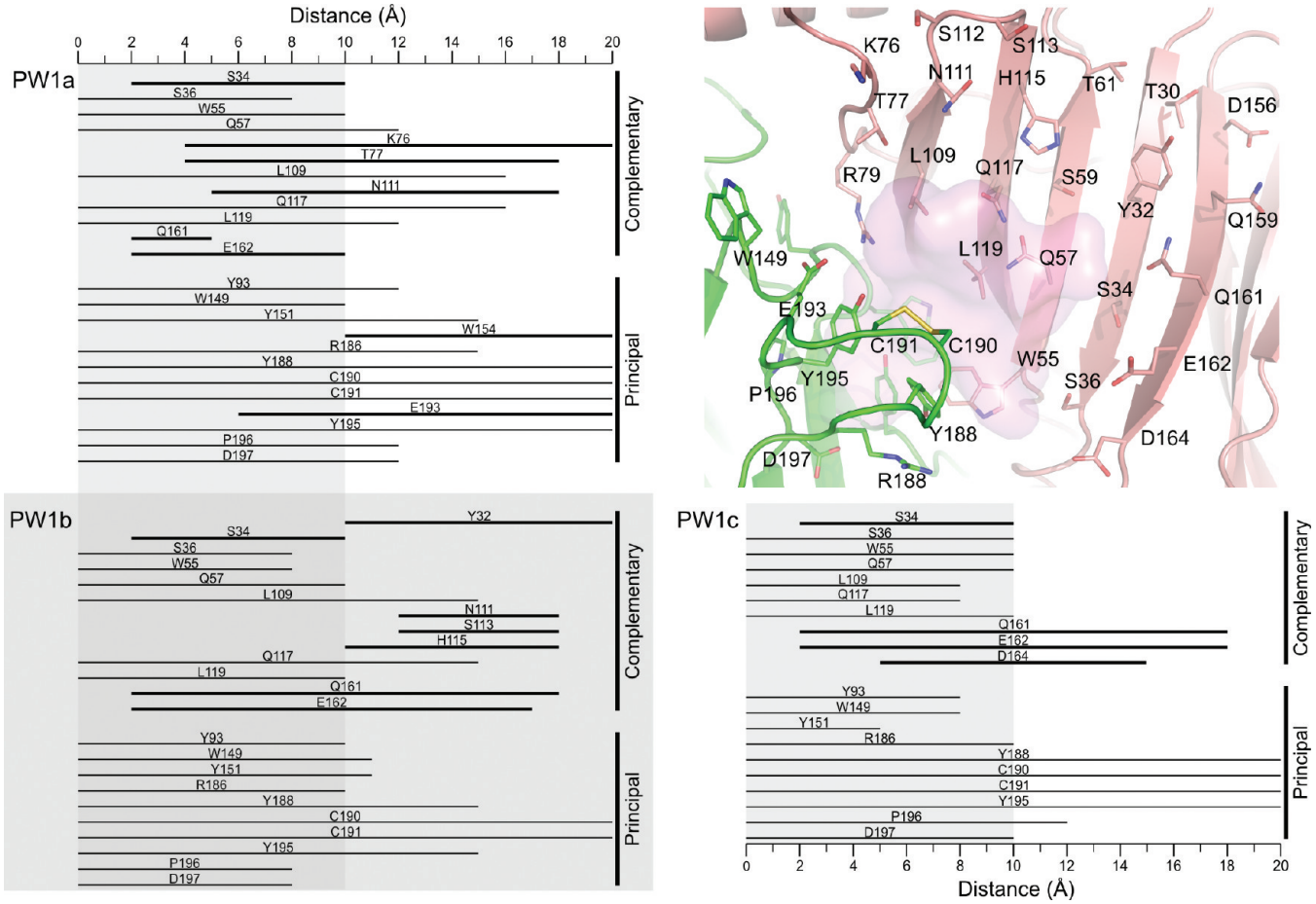

Figure 7. Positions of the receptor α7-nAChR in contact with ImI in the unbinding subpathways PW1a, PW1b, and PW1c sampled by steered molecular dynamics (SMD) simulations. For each subpathway, lines represent the involvement of each position at the interface with ImI. Bolder lines indicate positions that were not involved at the interface in the binding site. The reaction coordinate used on the *x*-axis is the distance between the initial position and the position during the simulation of the center of mass of ImI. In the top-right corner, α7-nAChR positions are highlighted on the initial conformation on the principal subunit (green) and complementary subunit (pink). ImI is represented using a violet transparent surface.

PW1b, and therefore, according to our computation, PW1c should be more frequently sampled than PW1b.

Pairwise interactions that have long-lasting participation in the two most probable pathways were identified. As shown in Figure S2, Supporting Information, all ImI positions had a similar number of interactions in the PW1b and PW1c simulations, except ImI-P6, which showed a higher number of contacts in PW1b than in PW1c. In the binding site, i.e., below 10 Å, ImI-P6 was embedded in a hydrophobic pocket formed by W55, Y92, L119, and W149 in PW1b and PW1c. At the end of the simulation, P6 mainly interacted with Y32, S113, H115, and Q161 in PW1b, and with Q161 and E162 in PW1c. ImI-R7 is the only residue displaying more interactions at the interface than P6. R7 constantly had the highest number of interactions at the interface in all simulations. ImI-R7 was in contact with Y195 in the binding pocket and formed a cation$-\pi$ interaction in both PW1b and PW1c after ImI had left its initial position. This cation$-\pi$ interaction has been predicted to exist in an experimental mutant cycle analysis.[15] The cation$-\pi$ interaction was formed in our simulations around 8 Å and was stable until 20 Å in some of the simulations. This long duration probably reflects the high strength of cation$-\pi$ interactions.[66] In addition to interacting with Y195, the side chain of R7 also established hydrogen bonds and charge interactions with D197 in both subpathways. The R7/D197 interactions occurred over the first 8 Å in PW1b and were maintained until the end of the simulation in PW1c. ImI-S4 was also significantly involved at the interface in PW1b and PW1c. Interestingly, ImI-S4 increased its contribution to the interface between 0 and 2 Å by contacting S34 and Q57. Both E162 and Q57 have been identified experimentally as influencing ImI binding.[15] In addition, ImI-S4 forms hydrogen bonds with E162 in PW1b and with D164 in PW1c from 7 to 15 Å. E162 and D164 also create hydrogen bonds and charge interactions with ImI-G1 around 10 Å, indicating that these two positions might be important to guide ImI during unbinding. Interestingly, experimental evidence shows that E162 and D164 are involved in the binding and unbinding of ImI.[15] Among the four positions in the first loop of ImI, ImI-D5 is the only position that is not extensively involved at the interface. The conformation of D5 is stabilized by interactions with other positions of ImI, especially by hydrogen bonds and charge interactions with R7. Generally, positions in the second loop of ImI have fewer interactions at the interface than positions in the first loop. ImI-A9 only participated in the interface until ImI was 10 Å from the binding site, and A9 was mainly involved in van der Waals interactions with L109 and Q117. Despite their relatively bulky side chain, ImI-W10 and ImI-R11 only create a few, nonspecific interactions at the interface.

dx.doi.org/10.1021/jp301352d | J. Phys. Chem. B 2012, 116, 6097−6105

4. CONCLUSIONS

Three main unbinding pathways of α-conotoxin ImI from the extracellular domain of the α7-nAChR were identified using RAMD simulations. On the basis of minimal conformational deformations, one pathway was considered the most probable and was further divided into three subpathways, which were investigated using SMD simulations. Using previous experimental mutation studies and PMF calculations, the two subpathways that are parallel and 45° to the membrane plane were identified as more probable. Interestingly, acetylcholine has also been proposed in a previous study to take a route parallel to the membrane,[60] and several interactions potentially important for the modulation of ImI activity were identified. ImI-R7 continually made the highest number of contacts at the binding interface with the α7-nAChR and was involved in a cation−π interaction with α7-Y195 and hydrogen bonds and charge interactions with α7-D197 in the SMD simulations. Receptor residues α7-E162 and α7-D164 also seemed to be important, as they were hydrogen bonded with both ImI-G1 and ImI-S4. Finally, some residues of ImI, including W10 and R11, have limited interactions with the α7-nAChR during unbinding and could probably be mutated without influencing the unbinding kinetics. Overall, the interactions identified in this study could be generally important for the rational drug design of a wide range of α-conotoxins because most conotoxins belonging to this pharmacological class display the same fold.

■ ASSOCIATED CONTENT

Supporting Information

Root-mean-square deviation (rmsd) of conotoxin ImI in subpathways PW1a, PW1b, and PW1c of the unbinding of ImI from α7-nAChR sampled by steered molecular dynamics (SMD); evolution of the number of pairwise atom contacts between conotoxin ImI positions and α7-nAChR positions in the subpathways PW1b and PW1c sampled by SMD simulations; potential of mean force (PMF) calculated in subpathway PW1b using linear extrapolation (in blue) and cumulative integral extrapolation (in red) methods applied to ten SMD simulations with a pulling speed of 5 Å·ns^{-1} or to ten SMD simulations carried out until the unbinding distance reached 30 Å. This material is available free of charge via the Internet at http://pubs.acs.org.

■ AUTHOR INFORMATION

Corresponding Author

*E-mail: d.craik@imb.uq.edu.au.

Author Contributions

‡These authors contributed equally to this work.

Notes

The authors declare no competing financial interest.

■ ACKNOWLEDGMENTS

This work was supported by a grant from the Australian Research Council (ARC DP1093115) and from the National Health and Medical Research Council (631457). We gratefully acknowledge access to the facilities of the ARC Special Research Centre for Functional and Applied Genomics. D.J.C. is a National Health and Medical Research Council Professorial Fellow (Grant ID APP1026501).

■ REFERENCES

(1) Terlau, H.; Olivera, B. M. *Physiol. Rev.* **2004**, *84*, 41−68.
(2) Azam, L.; McIntosh, J. M. *Acta Pharmacol. Sin.* **2009**, *30*, 771−783.
(3) Dutton, J. L.; Craik, D. J. *Curr. Med. Chem.* **2001**, *8*, 327−344.
(4) McIntosh, J. M.; Yoshikami, D.; Mahe, E.; Nielsen, D. B.; Rivier, J. E.; Gray, W. R.; Olivera, B. M. *J. Biol. Chem.* **1994**, *269*, 16733−16739.
(5) Johnson, D. S.; Martinez, J.; Elgoyhen, A. B.; Heinemann, S. F.; McIntosh, J. M. *Mol. Pharmacol.* **1995**, *48*, 194−199.
(6) Ellison, M.; Gao, F.; Wang, H.-L.; Sine, S. M.; McIntosh, J. M.; Olivera, B. M. *Biochemistry* **2004**, *43*, 16019−16026.
(7) Nicke, A.; Loughnan, M. L.; Millard, E. L.; Alewood, P. F.; Adams, D. J.; Daly, N. L.; Craik, D. J.; Lewis, R. J. *J. Biol. Chem.* **2003**, *278*, 3137−3144.
(8) Craik, D. J.; Adams, D. J. *ACS Chem. Biol.* **2007**, *2*, 457−468.
(9) Halai, R.; Craik, D. J. *Nat. Prod. Rep.* **2009**, *26*, 526−536.
(10) Carstens, B. B.; Clark, R. J.; Daly, N. L.; Harvey, P. J.; Kaas, Q.; Craik, D. J. *Curr. Pharm. Des.* **2011**, *17*, 4242−4253.
(11) Quiram, P. A.; Sine, S. M. *J. Biol. Chem.* **1998**, *273*, 11007−11011.
(12) Maslennikov, I. V.; Shenkarev, Z. O.; Zhmak, M. N.; Ivanov, V. T.; Methfessel, C.; Tsetlin, V. I.; Arseniev, A. S. *FEBS Lett.* **1999**, *444*, 275−280.
(13) Gehrmann, J.; Daly, N. L.; Alewood, P. F.; Craik, D. J. *J. Med. Chem.* **1999**, *42*, 2364−2372.
(14) Rogers, J. P.; Luginbühl, P.; Shen, G. S.; McCabe, R. T.; Stevens, R. C.; Wemmer, D. E. *Biochemistry* **1999**, *38*, 3874−3882.
(15) Quiram, P. A.; Jones, J. J.; Sine, S. M. *J. Biol. Chem.* **1999**, *274*, 19517−19524.
(16) Lamthanh, H.; Jegou-Matheron, C.; Servent, D.; Ménez, A.; Lancelin, J. M. *FEBS Lett.* **1999**, *454*, 293−298.
(17) Armishaw, C. J.; Daly, N. L.; Nevin, S. T.; Adams, D. J.; Craik, D. J.; Alewood, P. F. *J. Biol. Chem.* **2006**, *281*, 14136−14143.
(18) Armishaw, C.; Jensen, A. A.; Balle, T.; Clark, R. J.; Harpsøe, K.; Skonberg, C.; Liljefors, T.; Strømgaard, K. *J. Biol. Chem.* **2009**, *284*, 9498−9512.
(19) Yu, R.; Craik, D. J.; Kaas, Q. *PLoS Comput. Biol.* **2011**, *7*, e1002011.
(20) Romanelli, M. N.; Gratteri, P.; Guandalini, L.; Martini, E.; Bonaccini, C.; Gualtieri, F. *ChemMedChem* **2007**, *2*, 746−767.
(21) Taly, A.; Corringer, P.-J.; Guedin, D.; Lestage, P.; Changeux, J.-P. *Nat. Rev. Drug Discovery* **2009**, *8*, 733−750.
(22) Curzon, P.; Anderson, D. J.; Nikkel, A. L.; Fox, G. B.; Gopalakrishnan, M.; Decker, M. W.; Bitner, R. S. *Neurosci. Lett.* **2006**, *410*, 15−19.
(23) Wehner, J. M.; Keller, J. J.; Keller, A. B.; Picciotto, M. R.; Paylor, R.; Booker, T. K.; Beaudet, A.; Heinemann, S. F.; Balogh, S. A. *Neuroscience* **2004**, *129*, 11−24.
(24) Keller, J. J.; Keller, A. B.; Bowers, B. J.; Wehner, J. M. *Behav. Brain Res.* **2005**, *162*, 143−152.
(25) Unwin, N. *J. Mol. Biol.* **2005**, *346*, 967−989.
(26) Arias, H. R. *Neurochem. Int.* **2000**, *36*, 595−645.
(27) Dutertre, S.; Ulens, C.; Büttner, R.; Fish, A.; van Elk, R.; Kendel, Y.; Hopping, G.; Alewood, P. F.; Schroeder, C.; Nicke, A.; et al. *EMBO J.* **2007**, *26*, 3858−3867.
(28) Babakhani, A.; Talley, T. T.; Taylor, P.; McCammon, J. A. *Comput. Biol. Chem.* **2009**, *33*, 160−170.
(29) Hansen, S. B.; Sulzenbacher, G.; Huxford, T.; Marchot, P.; Taylor, P.; Bourne, Y. *EMBO J.* **2005**, *24*, 3635−3646.
(30) Le Novère, N.; Grutter, T.; Changeux, J.-P. *Proc. Natl. Acad. Sci. U.S.A.* **2002**, *99*, 3210−3215.
(31) Nyce, H. L.; Stober, S. T.; Abrams, C. F.; White, M. M. *Biophys. J.* **2010**, *98*, 1847−1855.
(32) Khatri, A.; Weiss, D. S. *J. Physiol.* **2010**, *588*, 59−66.
(33) Lummis, S. C. R.; Harrison, N. J.; Wang, J.; Ashby, J. A.; Millen, K. S.; Beene, D. L.; Dougherty, D. A. *ACS Chem. Neurosci.* **2012**, *3*, 186−192.

(34) Tsetlin, V.; Kuzmin, D.; Kasheverov, I. *J. Neurochem.* **2011**, *116*, 734−741.
(35) Thompson, A. J.; Padgett, C. L.; Lummis, S. C. R. *J. Biol. Chem.* **2006**, *281*, 16576−16582.
(36) Law, R. J.; Henchman, R. H.; McCammon, J. A. *Proc. Natl. Acad. Sci. U.S.A.* **2005**, *102*, 6813−6818.
(37) Saladino, A. C.; Xu, Y.; Tang, P. *Biophys. J.* **2005**, *88*, 1009−1017.
(38) Corry, B. *Biophys. J.* **2006**, *90*, 799−810.
(39) Brannigan, G.; Hénin, J.; Law, R.; Eckenhoff, R.; Klein, M. L. *Proc. Natl. Acad. Sci. U.S.A* **2008**, *105*, 14418−14423.
(40) Dougherty, D. A. *Chem. Rev.* **2008**, *108*, 1642−1653.
(41) Cederholm, J. M. E.; Schofield, P. R.; Lewis, T. M. *Eur. Biophys. J.* **2009**, *39*, 37−49.
(42) Forman, S. A.; Miller, K. W. *Can. J. Anaesth.* **2011**, *58*, 191−205.
(43) Lüdemann, S. K.; Lounnas, V.; Wade, R. C. *J. Mol. Biol.* **2000**, *303*, 797−811.
(44) Grubmüller, H.; Heymann, B.; Tavan, P. *Science* **1996**, *271*, 997−999.
(45) Balsera, M.; Stepaniants, S.; Izrailev, S.; Oono, Y.; Schulten, K. *Biophys. J.* **1997**, *73*, 1281−1287.
(46) Cuendet, M. A.; Michielin, O. *Biophys. J.* **2008**, *95*, 3575−3590.
(47) Cuendet, M. A.; Zoete, V.; Michielin, O. *Proteins* **2011**, *79*, 3007−3024.
(48) Morfill, J.; Neumann, J.; Blank, K.; Steinbach, U.; Puchner, E. M.; Gottschalk, K.-E.; Gaub, H. E. *J. Mol. Biol.* **2008**, *381*, 1253−1266.
(49) Neumann, J.; Gottschalk, K.-E. *Biophys. J.* **2009**, *97*, 1687−1699.
(50) Humphrey, W.; Dalke, A.; Schulten, K. *J. Mol. Graphics* **1996**, *14*, 33−38.
(51) Feller, S. E.; Zhang, Y.; Pastor, R. W.; Brooks, B. R. *J. Chem. Phys.* **1995**, *103*, 4613.
(52) Sagui, C.; Darden, T. A. *Annu. Rev. Biophys. Biomol. Struct.* **1999**, *28*, 155−179.
(53) Phillips, J. C.; Braun, R.; Wang, W.; Gumbart, J.; Tajkhorshid, E.; Villa, E.; Chipot, C.; Skeel, R. D.; Kalé, L.; Schulten, K. *J. Comput. Chem.* **2005**, *26*, 1781−1802.
(54) MacKerell, A. D., Jr.; Bashford, D.; Bellott, M.; Dunbrack, R. L., Jr.; Evanseck, J. D.; Field, M. J.; Fischer, S.; Gao, J.; Guo, H.; Ha, S.; et al. *J. Phys. Chem. B* **1998**, *102*, 3586−3616.
(55) Vashisth, H.; Abrams, C. F. *Biophys. J.* **2008**, *95*, 4193−4204.
(56) Park, S.; Khalili-Araghi, F.; Tajkhorshid, E.; Schulten, K. *J. Chem. Phys.* **2003**, *119*, 3559−3567.
(57) Jarzynski, C. *Phys. Rev. Lett.* **1997**, *78*, 2690−2693.
(58) Jarzynski, C. *Phys. Rev. E* **1997**, *56*, 5018−5366.
(59) Jarzynski, C. *Annu. Rev. Condens. Matter Phys.* **2011**, *2*, 329−351.
(60) Zhang, D.; Gullingsrud, J.; McCammon, J. A. *J. Am. Chem. Soc.* **2006**, *128*, 3019−3026.
(61) Ytreberg, F. M.; Zuckerman, D. M. *J. Comput. Chem.* **2004**, *25*, 1749−1759.
(62) Connolly, M. L. *Science* **1983**, *221*, 709−713.
(63) Winn, P. J.; Lüdemann, S. K.; Gauges, R.; Lounnas, V.; Wade, R. C. *Proc. Natl. Acad. Sci. U.S.A.* **2002**, *99*, 5361−5366.
(64) Schleinkofer, K.; Sudarko; Winn, P. J.; Lüdemann, S. K.; Wade, R. C. *EMBO Rep.* **2005**, *6*, 584−589.
(65) Wang, T.; Duan, Y. *J. Am. Chem. Soc.* **2007**, *129*, 6970−6971.
(66) Dougherty, D. A. *Science* **1996**, *271*, 163−168.